MAUSAM, **74**, 2 (April, 2023), 273-286

MAUSAM

DOI : https://doi.org/10.54302/mausam.v74i2.6000
Homepage: https://mausamjournal.imd.gov.in/index.php/MAUSAM

UDC No. 551.553.21 : 551.515.2

Decadal-scale changes in the seasonal transition patterns of the Asian summer monsoon and the South China Sea tropical cyclone frequency during May

MONG-MING LU, YIN-MIN CHO and CHUNG-HSIUNG SUI

Department of Atmospheric Sciences, National Taiwan University, Taiwan

e mail : mongminglu@ntu.edu.tw

सार – पश्चिमी उत्तरी प्रशांत (WNP) और दक्षिण चीन सागर (SCS) पर एशियाई ग्रीष्मकालीन मॉनसून की दशकीय-स्तर की विविधता तथा उष्णकटिबंधीय चक्रवातीय (TC) गतिविधि में बदलाव महत्वपूर्ण रूप से वैज्ञानिक और सामाजिक महत्व के हैं। 2010-2019 की अवधि को मई के दौरान दक्षिण चीन सागर और फिलीपीन सागर (cho *et al*., 2022) में उष्णकटिबंधीय चक्रवात के बनने के संबंध में 1961 के बाद से सबसे निष्क्रिय दशक के रूप में पहचाना गया था। इस लेख में हमने मई में दक्षिण चीन सागर में उष्णकटिबंधीय चक्रवात की आवृत्ति और एशियाई मॉनसून प्रणालियों के वसंत-से-ग्रीष्म में संक्रमण के बीच के संबंध को स्पष्ट करने के लिए 40-वर्षों (1981-2020) केडेटा का उपयोग करके विश्लेषण किया है। प्राप्तस परिणाम 1980 और 2000 के दशक के दौरान दो सक्रिय दशकों और 1990 और 2010 के दौरान दो निष्क्रिय दशकों के साथ उष्णकटिबंधीय चक्रवात की आवृत्ति की विशेष दशकीय-स्तर की विविधता दिखाते हैं। पहले के दो दशकों के दौरान परिसंचरण और सतही हवा के तापमान का अंतर बाद के दो दशकों से अत्यधिक भिन्न है। इस अंतर को एशियाई-ऑस्ट्रेलियाई-प्रशांत मॉनसून क्षेत्र में 40-वर्ष केमार्च-जून की वर्षा को दो प्रमुख तरीकों के दशकीय-स्तर की विविधता के रूप में समझा जा सकता है। पहले दो दशकों के लिए दक्षिण चीन सागर में उष्णयकटिबंधीय चक्रवात की आवृत्ति के विरोधाभाष को मई में हुई सक्रिय और निष्क्रिय विषमता को EOF2 में अंतर से समझाया जा सकता है। सकारात्मक EOF2 समवर्ती विसंगतियों के एक गीले और सूखे द्विध्रुवीय पैटर्न से मेल खाता है, जिसमें पूर्वी हिंद महासागर पर संवर्धित संवहन और पश्चिमी प्रशांत के उष्णक्षेत्र में संवहन कम हुआ है। बाद के दो दशकों के लिए, इसके विरोधाभास को EOF1 में अंतर से समझाया जा सकता है, जो ITCZ के उत्तरी गतिमानको दर्शाते हुए पूर्वी हिंद महासागर के ऊपर एक रेखांशिक द्विध्रुवीय पैटर्न को दर्शाता है। चार दशकों के बीच, 2001-2010 का दशक ITCZ के सबसे पहले उत्तर की ओर संक्रमण और मई में सबसे सक्रिय दक्षिण चीन सागर उष्णीकटिबंधीय चक्रवात आवृत्ति को दर्शाता है। हालांकि 1981-1990 और 1991-2000 के दशक उष्णयकटिबंधीय चक्रवात की आवृत्ति में अत्यधिक अंतर दिखाते हैं, मॉनसून ऋतु संक्रमण में कोई विशेष अंतर नहीं पाया गया है।

ABSTRACT. The decadal-scale variations of the Asian summer monsoon and the tropical cyclone (TC) activity over the western North Pacific (WNP) and the South China Sea (SCS) are of great scientific and societal importance. The period of 2010-2019 was identified as the most inactive decade since 1961 in terms of TC genesis over the SCS and the Philippine Sea during May (Cho *et al*., 2022). In this paper we extended the analysis by using 40-yr (1981-2020) data to illustrate the relationship between the SCS TC frequency in May and the spring-to-summer transition of Asian monsoon systems. The results show clear decadal-scale variations of TC frequency with two active decades during the 1980s and 2000s and two inactive decades during the 1990s and 2010s. The circulation and surface air temperature contrast during the earlier two decades is drastically different from the contrast during later two decades. The difference can be understood as decadal-scale variations of two leading modes of the 40-yr March-June precipitation in Asian-Australian-Pacific monsoon region. For the two earlier decades, the contrast of active and inactive SCS TC frequency in May can be explained by the difference in EOF2. The positive EOF2 corresponds to a wet and dry dipole pattern of the concurrent anomalies with enhanced convection over the eastern Indian Ocean and suppressed convection over the western Pacific warm pool. For the two later decades, the contrast can be explained by the difference in EOF1, which shows a meridional dipole pattern over eastern Indian Ocean reflecting the northward movement of the ITCZ. Among four decades, the decade of 2001-2010 shows the earliest northward transition of the ITCZ and the most active SCS TC frequency in May. Although the decades of 1981-1990 and 1991-2000 show strong difference in TC frequency, no discernable difference in monsoon seasonal transition is detected.

Key words – Asian monsoon, South China Sea monsoon, Indo-Pacific climate variability, Tropical cyclone.

1. Introduction

The vast Asian summer monsoon system extends from the Indian sub-continent eastward to Southeast and East Asia and further eastward to the Indo-Pacific maritime continent. An important feature of the monsoon system is the two-phase rainy season onset sequence (Wang and Linho, 2002). The first phase is referred to the onset of the rainy season over South and Southeast Asia in early- and mid-May. The second phase is referred to the onset of the rainy season of the grand Asian monsoon region in mid- and late-June. When the onset of the persistent rainy season occurs over the South China Sea (SCS) in mid-May, it signifies the completement of the first stage of the spring-to-summer transition of the Asian monsoon system. The first stage transition includes the establishment of a planetary-scale monsoon rainband that extends from the Arabian Sea (ArS), through India to the Bay of Bengal (BOB) and the SCS. The establishment of the rain belts over Taiwan, southern China and Okinawa region also occurs during the first stage of the transition around mid-May and usually persists for one month until mid-June (Cho and Lu, 2021). The second stage of the transition is characterized by a northwestward movement of the rainband associated with the second phase onset of the continental Indian rainy season, the establishment of Chinese Mei-yu and the Japanese baiu during the period from mid-June to mid-July and the Korean Peninsula and north-eastern China during mid-July to mid-August (Lau, 1992; Wang *et al*., 2001; Ding and Chan, 2005; Ding *et al*., 2020).

The spring-to-summer transition of the Asian monsoon system have been vigorously studied for many decades (Lu *et al*., 2020; Chen *et al*., 2019; Ding *et al*., 2015 and the references therein). The interdecadal variations of the transition has attracted great research interest. The mid-1990s has been identified as a significant change point in the onset time of the first stage transition (Kajikawa and Wang, 2012; Yuan and Chen, 2013; Chen, 2015; Wang and Kajikawa, 2015; Liu *et al*., 2016; Lin and Zhang, 2020; Hu *et al*., 2022). Kajikawa *et al*. (2012) found an advanced trend of the monsoon onset time over the BOB and the western North Pacific (WNP) revealed in the trends of the Asian monsoon rainfall and water vapor flux during 1979-2008 on a monthly mean basis. They showed an increasing (decreasing) trend of the rainfall in May (June) along 10° N in association with the advanced monsoon onset. They attributed the advanced onset and weakening of early summer Southeast Asian monsoon and western North Pacific monsoon to the changing heat contrast between the Asian landmass and the tropical Indian Ocean. The changing heat contrast may be resulted from the increased dust aerosol loading along the Himalaya-Tibetan Plateau that can enhance the heating in the mid-upper troposphere and strengthen the meridional thermal contrast (Lau and Kim, 2006; Lau *et al*., 2006). On the other hand, a significant advance in the South China Sea summer monsoon (SCSSM) onset dates around 1993/94 was reported by Kajikawa and Wang (2012). They found that before the mid-1990s when the onset was relatively late the commencement of the summer convection over the SCS was primarily determined by the northward seasonal march of the ITCZ. After the mid-1990s when the onset was advanced for about two weeks the commencement of the SCS convection was enhanced by the northwestward-moving tropical disturbances from the equatorial western Pacific. The SCS and Philippine Sea SSTs also increased significantly after the mid-1990s. The number of TCs that passed through the SCS and Philippine Sea was about doubled during 1994-2008 compared with those occurring during 1979-93. They suggested that the advanced SCSSM onset is rooted in the decadal change of the SST over the equatorial western Pacific. In a later report, Xiang and Wang (2013) showed that the advanced monsoon onset also occurred over ArS and BOB after 1999. The results of their numerical experiments with an atmosphere-ocean coupled climate model suggested that the advanced Asian summer monsoon onset can be attributed to the shift to the grand La Niña-like climate mean state in the Pacific basin. The La Niña-like mean state is characterized by the enhanced equatorial Pacific SST zonal gradients that can enhance the westward propagating Rossby waves and its interaction with the asymmetric background mean states in the Indian Ocean (IO) and WNP. The wave and mean state interaction can enhance the east-west heating contrast between the WNP and IO and further enhance the Northern Hemispheric perturbations and westerly winds (Lyon *et al*., 2014). Therefore, they advocated that the advanced monsoon onset in the ArS and BOB is governed by the equatorial Pacific SST zonal gradients, while the advanced monsoon onset of the SCS is strongly influenced by the abrupt SST warming near the Philippine Sea. Liu *et al*. (2016) supported the view that the grand La Niña-like modulation on the spring tropical temperature can enhance the upper-level pumping effect over the SCS during the decade after 1993/94 (1994-2014) and lead to the advanced monsoon onset.

The decadal-scale changes in the pattern of spring-to-summer transition of the Asian monsoon system can be revealed by the extreme weather systems such as tropical cyclone activity and extreme rainfall over the SCS and Southeast Asia (Cho *et al*., 2022; Hu *et al*., 2022; Tu *et al*., 2011; Xu and Wang, 2014). Cho *et al*. (2022) found that the advanced trend of the monsoon onset time and the SCSSM onset date after the mid-1990s was clearly weakened after the second decade of the twenty-first

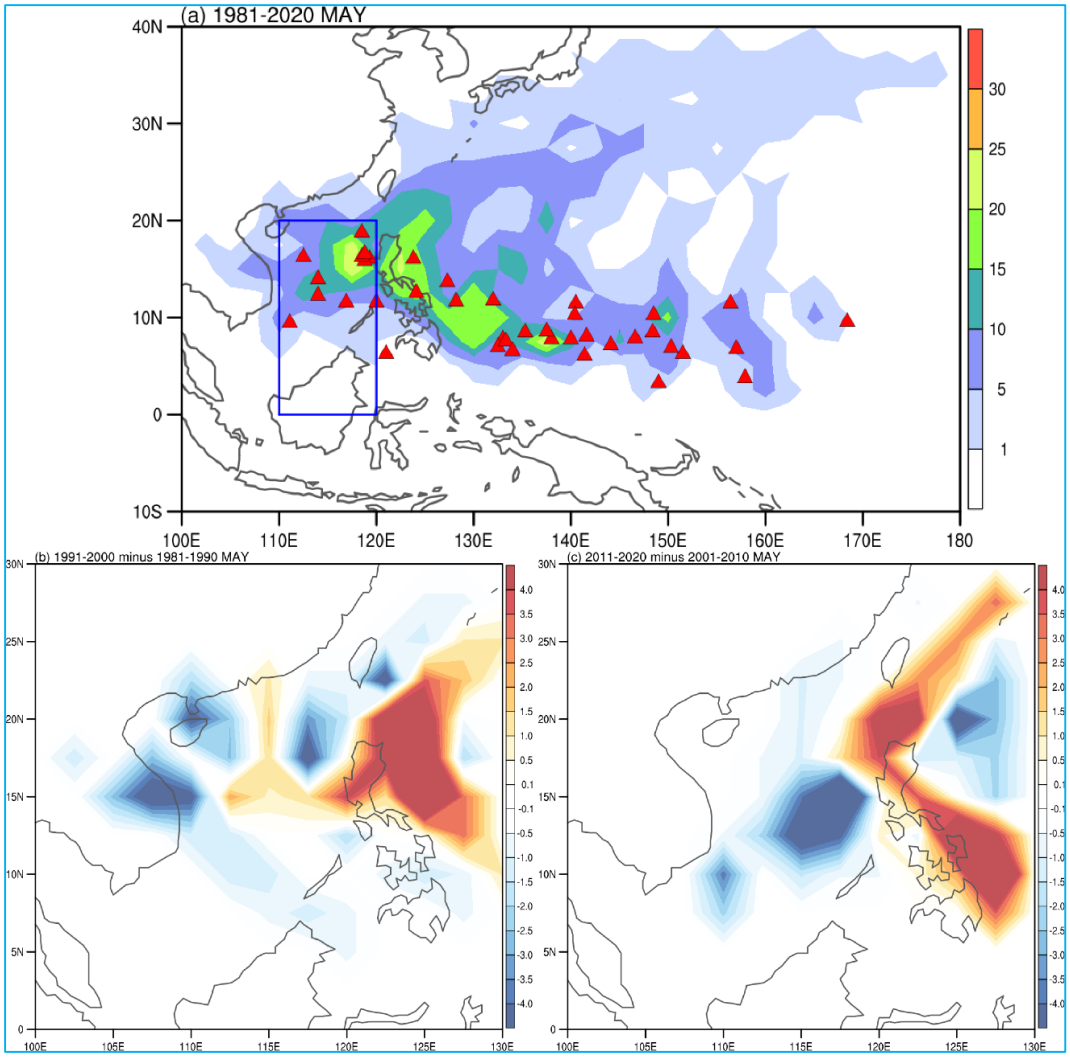

Figs. 1(a-c). (a) The accumulation of tropical cyclones (TC) passage frequency of each 2.5° × 2.5° grid area in May during 1981-2020. The TC genesis locations are indicated by the red triangles. The blue box indicates the South China Sea (SCS) regions (110° E-120° E, EQ - 20° N) for analysis of tropical cyclones. The TC passage frequency differences in May for the period of (b) 1991-2000 minus 1981-1990 and (c) 2011-2020 minus 2001-2010

century. The period of 2011-2020 was identified as a decade of the minimum TC genesis frequency over the SCS in May since 1961. The extremely inactive TC genesis was attributed to the weak low-level cross equatorial monsoonal flow over the Indo-Pacific warm pool and the weak westerly monsoon (easterly anomalies) north of the equator from the western Pacific through the Philippine Sea and the SCS to the Bay of Bengal. The weak tropical monsoon was associated with subtropical anticyclonic, the easterly anomalies to the south of 20° N and the westerly anomalies to the north of 20° N and the suppressed convection north of the equator associated with the opposite wind and convection south of the equator. The anomalous easterly was sustained by the enhanced SST gradient by the abnormally warm SST over the Indian Ocean and the anomalous westerly was associated with the cyclonic circulation and wet condition over the Asian continent.

Hu *et al.* (2022) found an early SCSSM onset tends to be accompanied by a higher chance of extreme rainfall over Southeast Asia, while a late SCSSM onset is likely to coincide with less heavy rainfall in May. The relationship was attributed to the difference in the amplitude of tropical synoptic-scale systems. After the SCSSM onset, the synoptic-scale environment becomes favorable to an anomalous cyclonic circulation over the SCS and Philippine Sea. It can moisturize the mid troposphere

through moisture advection and Ekman pumping and promote the barotropic instability and increase the intensity of the synoptic-scale systems. Tu *et al*. (2011) also suggested that the increased tropospheric water vapor in the mid-troposphere was a major factor for explaining more intense typhoons after 2000. Suffice it to say that the extreme rainfall and tropical cyclone frequency in May over the SCS are good indicators for understanding the variations of the spring-to-summer monsoon transition of the vast Asian monsoon system.

In this paper, we extend the analysis in Cho *et al*. (2022) (hereinafter referred to as CLS2022) by using 40 years (1981-2020) of data to illustrate the relationship between the SCS TC frequency in May and the spring-to-summer development of Asian monsoon systems. It was shown in Fig. 1(b) in CLS2022 that 1991-2000 is a decade with the least frequent TC genesis in the 6 decades (each decade has 10 successive years) since 1961, but did not analyze the similarity between the two weak TC decades of 1991-2000 and 2011-2020. In order to enhance the understanding on the decadal-scale changes of the Asian monsoon system, we separate the 40 years from 1981-2020 into four decades in the present study to document the contrast between the spring-to-summer transition of the active SCS May-TC decade and the inactive SCS May-TC decade [Fig. 3(a) in CLS2022]. A specific emphasis is placed on analyzing the similarity and differences in the contrast before and after the year 2000. The findings can be applied to improve climate monitoring and prediction, particularly in Southeast Asia.

The paper is arranged as follows. The data and methodology are described in section 2. The results and discussion presented in section 3 include three subsections that describe the SCS TC frequency variability during May, the climatological features of the spring-to-summer transition of the Asian monsoon system and the decadal-scale contrast of the seasonal transition. A summary and discussion of this study and conclusions are presented in Section 4. The results of this study can improve understanding of the relationship between regional climate, TC and the Asian-Pacific monsoon evolution during the monsoon transition period in early summer.

2. Data and methodology

2.1. *Data*

The large-scale climate data used in this study include the ECMWF Reanalysis v5 (ERA5) data (Hersbach *et al*., 2020), NASA's Global Precipitation Climatology Project (GPCP) version2.2 pentad rainfall data (Huffman *et al*., 2009) and the interpolated daily outgoing longwave radiation (OLR) version 1.2 with the spatial resolution of 1° × 1° (Lee, 2011). For SST data, the NOAA Extended Reconstructed Sea Surface Temperature (ERSST v5; Huang *et al*., 2017) of monthly and 2° × 2º horizontal resolution is used.

The TC data used in this study is the best track data produced by Regional Specialized Meteorological Center (RSMC), Tokyo, Japan (http://www.jma.go.jp/jma/jma-eng/jma-center/rsmc-hp-pub-eg/besttrack.html). The RSMC Tokyo-Typhoon Center maintains near real-time updates of the JMA TC best track data. TC in the present study refers to tropical storms and typhoons that have the maximum sustained wind speed of the surface wind (VMAX) of 34 knots or higher (wind speed > 34 knots) during the storm's entire lifetime. The TC genesis location is identified as the latitude and longitude of the first record of VMAX that exceeds 34 knots. The TC passage frequency maps are calculated at each pixel of the 2.5 × 2.5 degrees of latitude and longitude grid boxes.

2.2. *Methods*

The spring-to-summer transition discussed in CLS2022 is based on the monthly tendency of the large-scale circulation evolution calculated as the difference between later and earlier months or bi-month in two or four subsequent months from March to June. The northward movement of the precipitation centers in the regional monsoon sectors of ArS, BOB and SCS is also used for illustrating the seasonal transition. In the present study, we use the Empirical Orthogonal Function (EOF) analysis method to analyze the precipitation data over the Asian-Australian-Pacific monsoon region (40° E-180° E, 15° S-40° N) to objectively represent the seasonal transition.

The velocity potential and stream function presented in this study is calculated using spherical harmonics from NCAR Command Language (NCL) available athttps://www.ncl.ucar.edu/Document/Functions/spherical.shtml. (Boulder, Colorado: UCAR/NCAR/CISL/TDD. http://dx.doi.org/10.5065/D6WD3XH5)

3. Results and discussion

3.1. *SCS TC frequency during May*

Fig. 1(a) shows the geographical distribution of the WNP and SCS TC frequency in May based on 40-yr (1981-2020) TC data. TCs tend to form within a narrow zonal band from 5° N to 10° N over the western Pacific warm pool to the north of New Guinea from 130° E to 150° E. To the east of 150° E, TC genesis can occur to the south of 5° N, while to the west of 130° E the TC genesis on average occurred to the north of 10° N. In other words,

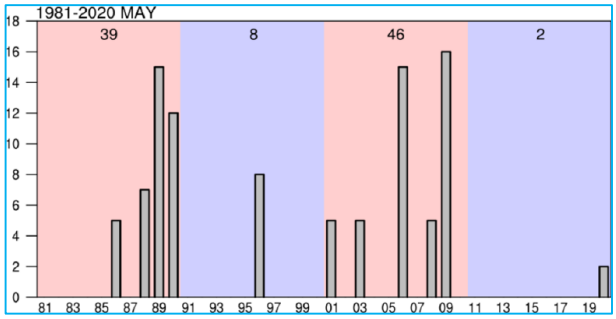

Fig. 2. TC frequency counted over the SCS region (110° E-120° E, EQ - 20° N) during May in the 6-hourly RSMC Best Track Data from 1981 to 2020. The numbers above the histogram represent the sums of TC frequency in four decades: the 1980s, 1990s, 2000s and 2010s

to the west of 130° E the TC genesis location is in general more north than those ones formed to the east of 130° E. The TC passage also shows different patterns to the east and west of the Philippines. To the east of 130° E, the TC passage orientation is very similar to the zonal feature of TC genesis, while to the east of 120° E the passage shows a southeast-northwest oriented narrow path near the Philippines but to the west of 130° E the passage shows a southwest-northeast oriented path from the SCS through the Bashi channel to the Pacific Ocean. To the east of the Philippines the TC passage shows a clear curve structure from, say, 140° E, 7° N over the west Pacific warm pool to the northern Philippine islands and then turn northeastward to the western North Pacific. The contrasts over the SCS and the Philippine Sea of TC passages and genesis are mainly caused by the low-level large-scale flows that is mainly southwesterly over the SCS and anticyclonic over the Philippine Sea. Fig. 3(a) in CLS2022 shows that before the year 2000 the decade of 1981-1990 is an active period with more frequent TC activity over the SCS in May, while the decade of 1991-2000 is an inactive period with less frequent TC activity. After the year 2000, it appears that the cycle was repeated with the decade of 2001-2010 active and the decade of 2011-2020 inactive. The difference in the TC passage decadal difference maps, the difference between the inactive and active decades, before and after the year 2000 is clearly shown in Figs. 1(b&c). Before the year 2000 [Fig. 1(b)], the less active decade shows lower TC frequency relative to the more active decade over western SCS near the coastal regions of Vietnam and Hainan and the northern SCS near Bashi Channel and Taiwan, while higher TC frequency over the northern Philippines and the western Philippine Sea. After the year 2000 [Fig. 1(c)], the lower TC frequency appears over the entire SCS, while the pattern of higher TC frequency resembles the high density TC passage in Fig. 1(a). Such pattern suggests that the TC formed over the SCS during the less frequent decade is much less than that during the more frequent decade.

The time series of the TC frequency over the SCS region in May presented in Fig. 2 suggest that the 40-year can be separated into two active and two inactive decades. The SCS area (110° E-120° E, EQ - 20° N) where the TC frequencies are counted is shown by the rectangular box in Fig. 1(a). Fig. 2 shows that the decades of 1981-1990 and 2001-2010 can be termed as the active SCS May-TC decades, while the decades of 1991-2000 and 2011-2020 can be termed as the inactive SCS May-TC decades. During the inactive decades, the total frequencies (unit : 1/6hr) of the SCS May-TC are 8 and 2 for the first and second decades, respectively. During the active decades of 1981-1990 and 2001-2010 total frequencies of the SCS May-TC are 39 and 46, respectively.

3.2. *Spring-to-summer transition*

The spring-to-summer transition of the Asian monsoon system can be best seen in the climatological precipitation and 850-hPa winds from 11 April - 9 June [Figs. 3(a-f)]. During the period from mid-April to early-May the precipitation is mainly over Indonesia maritime continent.

The equatorial rain is strongest during April and significantly weakened in mid-May when the Mei-yu front became intensified after mid-May, Over the western Pacific (130° E-170° E), the rainfall center gradually shifts westward from 160° E-170° E in April to 130° E-150° E in early-June. Over the subtropical region to the north of 10° N, a clear rain band oriented in the southwest-northeast direction significantly intensified during the transition period from mid-April to early-May.

We select seven strategic regions shown in the mid-April to early-June average precipitation and 850 hPa map [Fig. 3(g)] to illustrate the geographically difference in seasonal transition represented by the area mean precipitation. BOB, SCS and Taiwan-Okinawa represented by Box A, D and C respectively, are the areas with the largest amplitude of spring-to-summer rainfall transition. All three areas show an increasing trend of precipitation from mid-April to early-June. The peak precipitation of the western Indian Ocean (Box B) appears in mid-May (pentad 27-28) and then slightly drops in late-May followed by slight increases in early-June. Over Boneo Island (Box E), the seasonal transition tendency is opposite to the BOB and SCS, with a decreasing tendency from the mild peak in late-April (pentad 24-25) to a point of minimum precipitation in late-May (pentad 29). Over the southern Philippine Sea (Box F) and New Guinea island (Box G) regions, we see mild spring-to-summer rainfall variation. Fig. 3(m) (Box F) shows that the rainfall curve stays near 3 mm day-1 before pentad 25 (1-5 May), then a clear increasing trend after pentad 25 and reaches

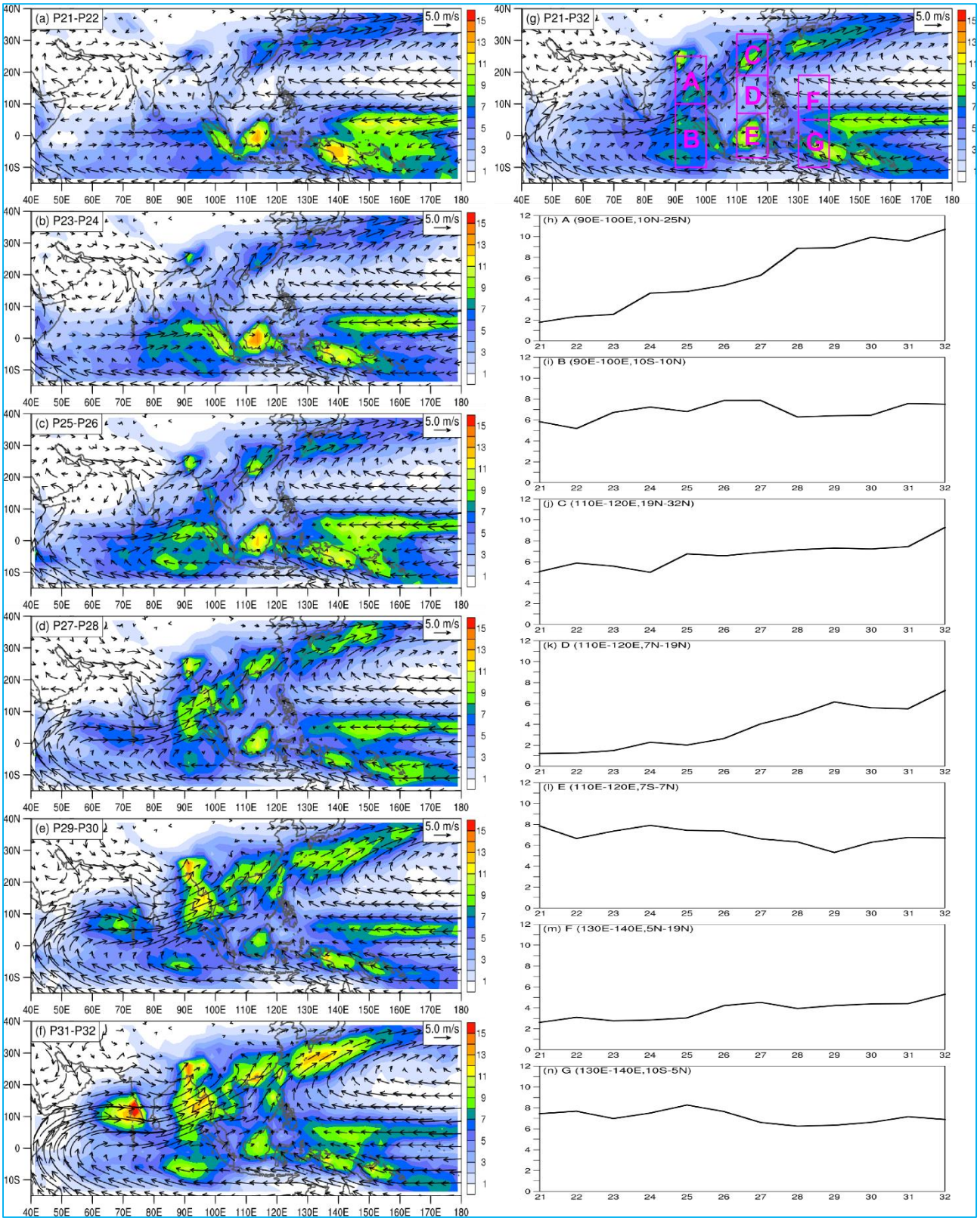

Figs. 3(a-n). Climatological mean precipitation (GPCP; shading, mm day^{-1}) and 850hPa winds (ERA5; vectors, ms^{-1}) for (a) pentad 21 to 22, (b) pentad 23 to 24, (c) pentad 25 to 26, (d) pentad 27 to 28, (e) pentad 29 to 30, (f) pentad 31 to 32, (g) pentad 21 to 32 over the period of 1981-2020 and (h)-(n) The time series of the climatological pentad mean rainfall over seven pink boxes in (g)

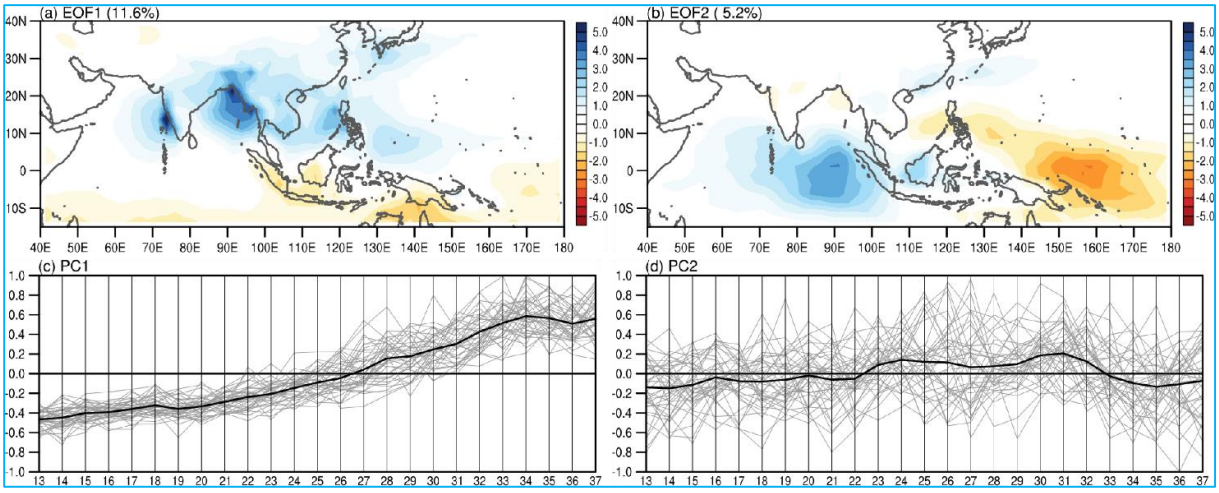

Figs. 4(a-d). The EOF analyses of March-June (pentad 13 to 37) GPCP precipitation during 1981-2020 over 40° E-180° E, 15°S-40° N. Spatial distribution of (a) the first mode (EOF1) and (b) the second mode (EOF2). The corresponding principle components (PCs) of (c) the first mode (PC1) and (d) the second mode (PC2). The black and grey curves indicate the time coefficients averaged for 1981-2020 and the time coefficients in each year, respectively

the maximum value at pentad 32 (5-9 June). Fig. 3(n) (Box G) shows a modest rainfall peak at pentad 25, then a small decreasing trend with a bump at pentad 31 (1-5 June). The opposite trend tendency reflects the tendency such as the precipitation systems become more active to the north of the equator and less active to the south of the equator as the boreal summer season sets in. The variation patterns of the time series suggest an interesting aspect of the regional contrast in the seasonal transition during the monsoon development stage in May.

The regional contrast in the seasonal transition can be captured by the two leading modes identified using the EOF analysis method applied to the March-June precipitation data over the Asian-Australian-Pacific monsoon region. The spatial pattern of EOF1 and its principal component (PC1) is shown in Figs. 4(a&c). It is evident that the EOF1 captures the northward movement of the ITCZ. The phase transition occurs around pentad 25-27 (1-15 May). Before the transition, the zonally oriented precipitation centers are mainly over the Indonesian maritime continent and the Timor and Arafura Seas and after the transition the precipitation centers are over ArS, BOB, SCS and Indochina Peninsula. Therefore, EOF1 captures the most robust seasonal transition associated with the northward movement of the ITCZ.

EOF2 shows an east-west contrast of the precipitation variation over the eastern Indian Ocean and western Pacific warm pool region. PC2 shows two nodes of the phase transition with the mean occurrence time of the first transition at pentad 22-23 (20-21 April) and the mean occurrence time of the second transition at pentad 32-34 (9-19 June). The occurrence time of the first transition is earlier than the first phase onset described in Wang and Linho (2002) and many other documents, while the second transition coincides with the second phase onset transition in Wang and Linho (2002) which is referred to the onset of the rainy season of the grand Asian monsoon region in mid-and late-June. The spatial pattern suggests a concurrent change over the eastern Indian Ocean and the western Pacific warm pool. Over the eastern Indian Ocean, the change is from dry to wet and over the western Pacific warm pool it is from wet to dry. Another interesting pattern is the positive-negative-positive precipitation anomaly pattern from Boneo northward to the SCS and to Taiwan-Okinawa. It suggests that the influence of the western Pacific subtropical high (WPSH) on the regional precipitation pattern is captured by EOF2. Associated with the spring-to-summer seasonal transition the WPSH is intensified from March to mid-June (Cho and Lu, 2017). Associated with the northward movement of the WPSH during mid- and late-June precipitation over the equatorial eastern Indian Ocean tends to become weaker and the precipitation over the SCS and western Pacific warm pool region tends to become stronger [Figs. 3(a-n)]. Therefore, EOF2 captures the seasonal transition patterns of the precipitation over the BOB, SCS and the Philippines Sea region. When the EOF2 is strong the SCSSM onset such as the dry-to-wet transition over the SCS in late-May [pentad 29-30, Fig. 3(k)] can be delayed. It is noted that PC2 shows large interannual and intraseasonal fluctuations compared with PC1. However, it is evident that during the critical period of the SCS summer monsoon onset from pentad 28 to pentad 32 (16 May-9 June) the PC2 shows strong

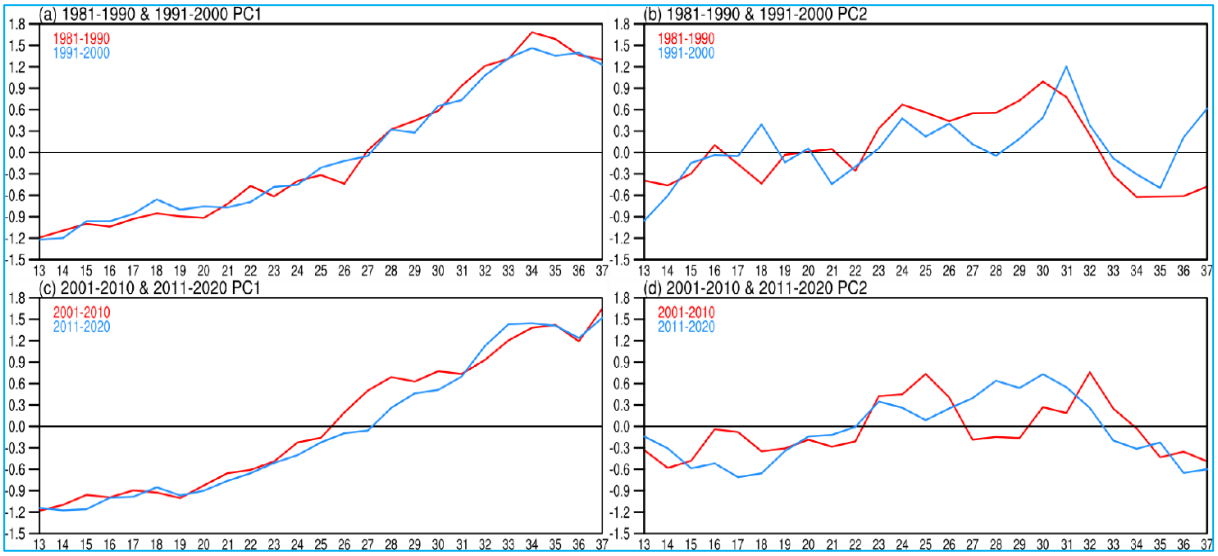

Figs. 5(a-d). The average of the time series of (a) PC1 and (b) PC2 for the period 1981-1990 (red curve) and 1991-2000 (blue curve). As in (a-b), (c-d) for the period 2001-2010 (red curve) and 2011-2020 (blue curve)

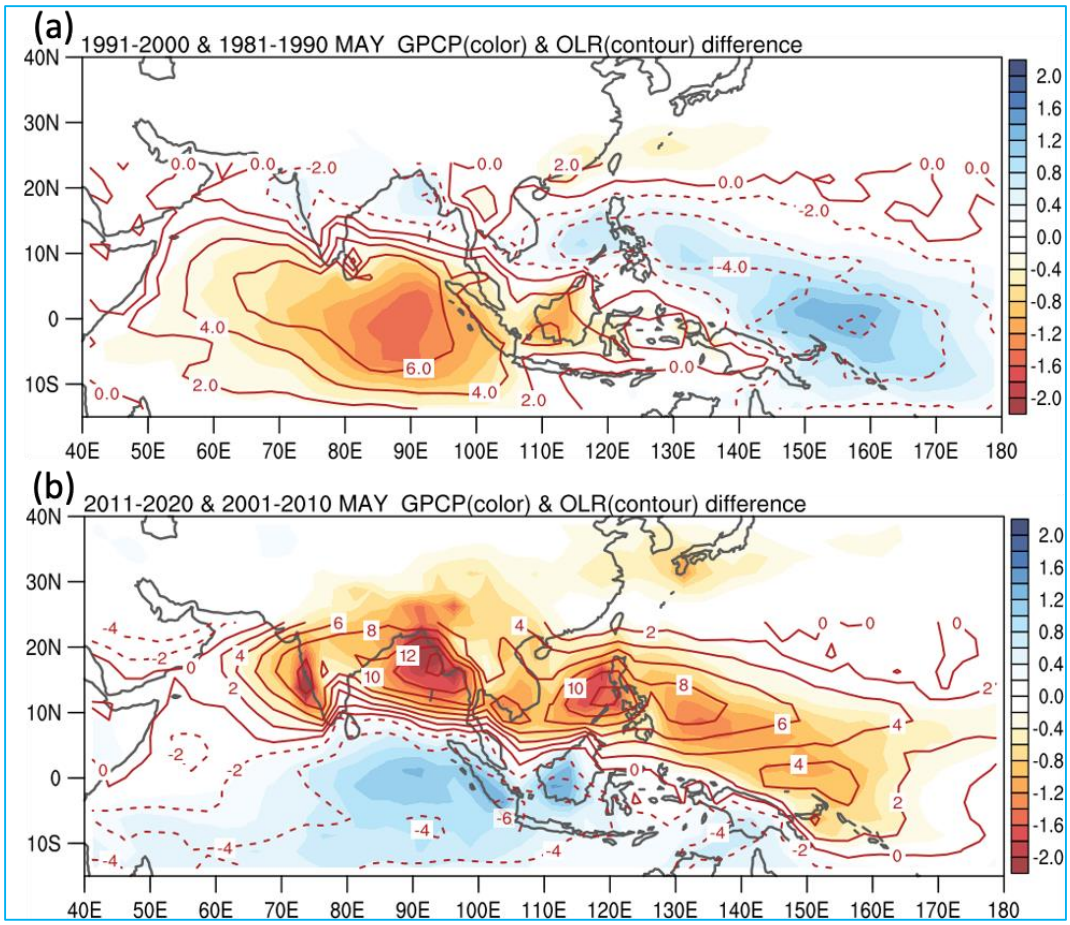

Figs. 6(a&b). The difference of the reconstructed precipitation based on the first two leading EOFs (GPCP; shading, mmday^{-1}) and the regressed OLR (NOAA; contours, Wm^{-2}) for the period of (a) 1991-2000 minus 1981-1990 and (b) 2011-2020 minus 2001-2010 in May. The contour interval is 2 Wm^{-2}

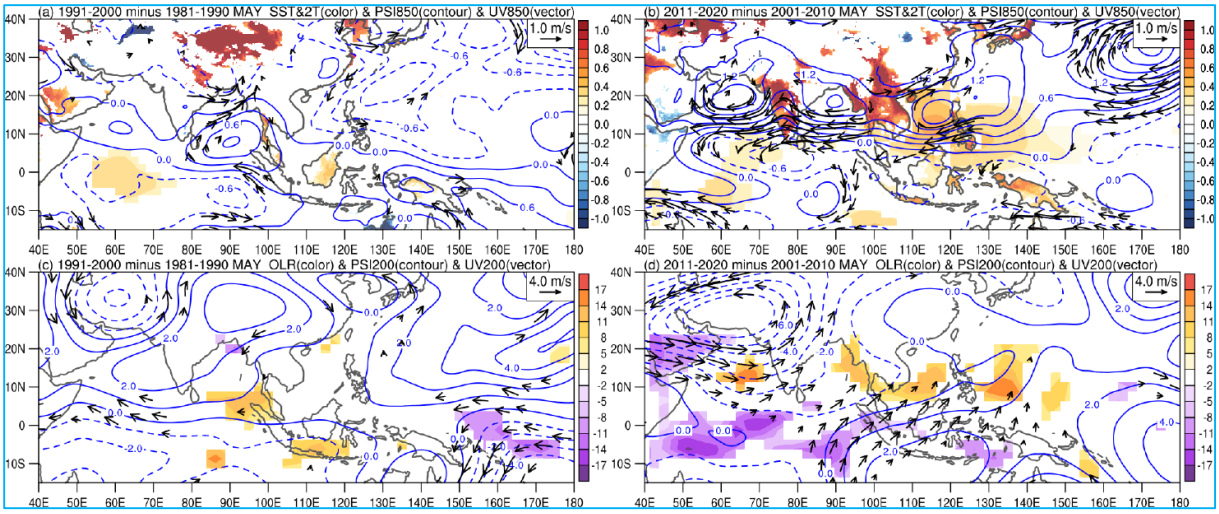

Figs. 7(a-d). The difference of SST (ERSSt; shading over ocean, °C), 2-meter air temperature (ERA5; shading over land, °C), 850 hPa stream function (ERA5; contours, m^2s^{-1} 10^6) and 850 hPa winds (ERA5; vectors, ms^{-1}) for the period of (a) 1991-2000 minus 1981-1990 and (b) 2011-2020 minus 2001-2010 in May. The contour interval is 0.3 $m^2s^{-1}10^6$. (c-d) As in (a-b), the difference of outgoing long-wave radiation (NOAA; shading, Wm^{-2}), 200 hPa stream function (ERA5; contours, m^2s^{-1} 10^6) and 200 hPa winds (ERA5; vectors, ms^{-1}). The contour interval is 1 $m^2s^{-1}10^6$. Except for the stream function field, the significance at the 90% confidence level is shown

positive tendency. This is a period of unusual strong climatological ISO cycle documented in Wang and Xu (1997) and will be discussed in Section 4.2.

3.3. *Decadal-scale contrast of the seasonal transition*

The focus of this section is to discuss the relationship between the monsoon transition and the SCS TC frequency in May. Interestingly, the 4 decades since 1981 consist of two decades of more active SCS May-TC, namely, 1981-1990 and 2001-2010 and two decades of less active SCS May-TC, namely, 1991-2000 and 2011-2020. The contrast offers a good opportunity for understanding how SCS May-TC frequency is associated with the seasonal transition of the monsoon system. Figs. 5(a-d) show the contrast between the more and less active SCS May-TC decades represented by PC1 and PC2. PC 1 corresponds to the northward movement of the ITCZ associated with the seasonal transition and PC2 corresponds to the westward movement of the center location of large precipitation associated with the seasonal transition and transient intraseasonal fluctuations. Before the year 2000, the movement of ITCZ (PC1) does not show any discernable difference between the active and inactive SCS May-TC decades. However, after the year 2000, the seasonal transition of more active decade (2001-2010) is more advanced than the transition of less active decade (2011-2020). This is consistent with previous studies (Kajikawa and Wang, 2012). The difference between the active and inactive decades before the year 2000 is discernable in PC2 during pentad 23-32 (21 April-9 June) [Fig. 5(b)]. The active decade (1981-1990) shows large and persistent positive PC2 from pentad 23 to pentad 32 (21 April-9 June), while the inactive decade (1991-2000) shows large intra-seasonal variability with the minimum amplitude of PC2 in pentad 28 (16-20 May). It suggests that the more active SCS May-TC may reflect the advanced monsoon transition associated with EOF2. The situation is reversed after the year 2000. The active decade (2001-2010) shows larger intra-seasonal variability with the prolonged weak PC2 during pentad 27-29 (11-25 May), while during the same period the inactive decade (2011-2020) shows large and persistently large positive PC2. It was discussed in CLS2022 that 2011-2020 is an unusually quiet decade for SCS TC genesis in May with the unusually strong anticyclone over the SCS in May.

This is consistent with the persistently large positive PC2 shown in Fig. 5(d). The TC frequency difference maps in Figs. 1(b&c) are consistent with the findings here such as before the year 2000, the difference between the active and inactive decades is mainly over the western SCS near the coastal regions of Vietnam and Hainan and the northern SCS near Bashi Channel and Taiwan, while after the year 2000 the difference is mainly over the central SCS. The opposite patterns between PC2 and the SCS May-TC frequency suggests that the spring-to-summer transition of regional monsoons can be influenced by the intra-seasonal variability of tropical convection and

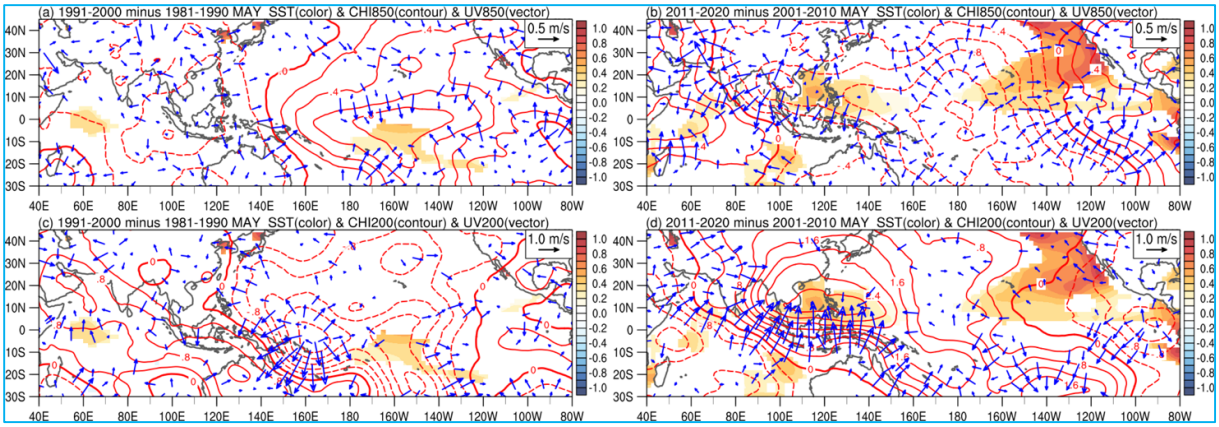

Figs. 8(a-d). The difference of SST (ERSSt; shading, °C), 850 hPa velocity potential (ERA5; contours, m^2s^{-1} 10^6) and 850 hPa winds (ERA5; vectors, ms^{-1}) for the period of (a) 1991-2000 minus 1981-1990 and (b) 2011-2020 minus 2001-2010 in May. The contour interval is 0.2 $m^2s^{-1}10^6$. (c-d) As in (a-b), but the contours is 200hPa velocity potential (ERA5; contours, m^2s^{-1} 10^6) and the vectors is 200 hPa winds (ERA5; vectors, ms^{-1}). The contour interval is 0.4 $m^2s^{-1}10^6$. Except for the velocity potential field, the significance at the 90% confidence level is shown

primary transition (EOF1) associated with the northward jump of the ITCZ.

The decadal-scale contrast in the monsoon transition can be further illustrated in Figs. 6(a&b) which shows the difference, the SCS May-TC inactive decade minus the active decades, in the reconstructed precipitation based on two leading EOFs and the regressed OLR during May. The contrast resembles the EOF1 and EOF2 patterns in Figs. 4(a-d) but of opposite signs. Note that the positive anomalies in Figs. 4(a-d) correspond to after the spring-to-summer transition as the PC time series represent. Therefore, Figs. 6(a&b) show that before year 2000 the EOF2 was a major component to explain the decadal-scale contrast in the seasonal transition, while after year 2000 the EOF1 was a major component.

Figs. 7(a-d) show the large-scale circulation and surface temperature differences associated with the decadal-scale contrast between the inactive and active decades. For the SST and wind vectors only the differences statistically significant at the 0.1 level are shown in the figures. The rather low 0.1 significance level reflects that before year 2000 the decadal-scale contrast was statistically weak. Despite the weak signal, it is interesting to see the emerged consistent structure of the scattered significant contrast in SST and wind when using the stream function to fill the void. The differences of 850-hPa winds, stream function and surface air temperature between the inactive and active decades before the year 2000 are presented in Fig. 7(a) and after year 2000 in Fig. 7(b). Completely different features before and after the year 2000 are evidently revealed. Before the year 2000, a southeast-northwest oriented positive stream function extended from the Coral Sea to the northwest through New Guinea and Indonesia maritime continent to the BOB and the southern ArS. The significant difference in 850-hPa winds only appears along the southern rim of the positive stream function. The strong southeasterly wind extended from the Timor Sea along the south coastal region of Sumatra toward the northwest and merged into the anticyclonic circulation over BOB. The circulation pattern suggests that for the precipitation systems to develop over the BOB, the large-scale environment during the decade of 1981-1990is more favorable than the decade of 1991-2000. The surface temperature over Tibetan Plateau is warmer during the inactive decade. At 200-hPa over the Tibetan Plateau, it shows that the inactive decade of 1991-2000 had stronger upper-level anticyclone over the Asia continent. The low-level westerly wind and upper-level anticyclone are not favorable for TC genesis over the SCS and for the WNP TCs to move westward into the SCS. An interesting low-level wind pattern in Fig. 7(a) appears over the western North Pacific between Okinawa and northern Philippines. Stronger cyclonic circulation during the decade of 1991-2000 is consistent with the May TC frequency contrast in Fig. 1(a). The anomalous northwesterly winds over northern SCS and the westerlies (associated with the negative stream function) over the Philippines prohibited the western North Pacific TCs to move into the SCS. The anomalous cyclonic circulation over the tropical western North Pacific can be enhanced by the warm SST anomaly in central equatorial Pacific [Fig. 8(a)] resembling the Matsuno-Gill like response to the SST forcing.TC genesis over the western North Pacific was more active during 1991-2000 and the large-scale condition is more favorable for turning toward extra tropical Pacific. The patterns of

the 850-hPa wind and stream function suggest that during the active decade (1981-1990) of SCS May-TC the BOB monsoon onset cyclone is more active in May which is a favorable condition for the onset of monsoon transition is encouraged to occur earlier.

After the year 2000, the contrast is drastically different. The zonally elongated positive OLR difference to the north of 10° N in Fig. 7(d) is striking. It covers the region from the ArS, BOB, the Indochina peninsula, the SCS, the Philippine Sea and further to the western Pacific and the Coral Sea in the Southern Hemisphere. To the south of the large positive OLR difference region, which shows a decadal-scale suppressed tendency of the tropical deep convection, is the negative OLR difference that covers the entire equatorial Indian Ocean, the Indonesia maritime continent and the Arafura Sea. Associated with the active convection over the eastern Indian Ocean to the south of Sumatra island, we see a large area of southerly winds blowing in the direction from the eastern South Indian Ocean (80° E-110° E, 10° S-15° S) crossing the equator to the Northern Hemisphere. Fig. 7(b) shows that at 850-hPa is a cyclonic (counterclockwise) circulation in association with the east-west elongated negative OLR belt from the western equatorial Indian Ocean extending southeastward to the Arafura Sea [Fig. 7(d)]. To the north of the cyclonic circulation is strong easterlies extending from the WNP through the SCS to the northern Indian Ocean. The strong easterlies suggest the decadal-scale weakening of the monsoonal westerly flow. Note that the low-level cyclonic winds over the western South Indian Ocean (40° E-90° E, 0°-10° S) [Fig. 7(b)] is associated with the enhanced convection represented by the negative OLR in Fig. 7(d) that resembles the ITCZ.

3.4. *Decadal-scale contrast of divergent circulation and precipitation*

The decadal contrast of the inactive and active SCS May-TC decades can be further illustrated by the 850-hPa and 200-hPa velocity potential and SST [Figs. 8(a-d)]. Before year 2000, the main divergent circulation differences between inactive and active decades can be summarized as follows. When the upper-level divergent center is enhanced over the west Pacific warm pool [Fig. 8(c)] the low-level divergence over the equatorial eastern Indian Ocean specifically to the southeast of Sumatra can be enhanced [Fig. 8(a)]. Thus, the development of tropical convective systems to the east of the Philippine, Indonesia and New Guinea islands are enhanced and to the west of the islands are suppressed. Note that the SSTs over central equatorial Pacific (180°-140° W, 10° S-0°) was warmer during the inactive decade, which induced stronger convergent flow and enhanced the ITCZ over the western Pacific. The decadal-scale SST contrast is enhanced during the decades after 2000. Fig. 8(b) shows that during the inactive decade of 2011-2020 the SSTs over eastern North Pacific is substantially warmer than the decade of 2001-2010. Over central equatorial Pacific the low-level divergent flow is stronger during 2011-2020, therefore, the western Pacific ITCZ is weaker. Over the South Indian Ocean near the equator the low-level convergent flow, the ITCZ and the upper-level divergence was enhance during 2011-2020. The SCS became a center of the enhanced low-level divergence, therefore the TC frequency dropped to the lowest in 60 years. Before 2000, the SCS May-TC frequency variation reflects the regional monsoon, in particular the transition over the BOB variations. After 2000, the SCS May-TC frequency variation reflects a much wider scale variations associated with the northward movement of the ITCZ over the western Pacific-Indian Ocean monsoon region.

4. Conclusions and discussion

4.1. *Summary*

The decadal-scale differences of the spring-to-summer transition of the vast Asian monsoon system has been analyzed with a focus on revealing the relationship between the TC frequency in May over the SCS and monsoon. The 4 decades since 1981 are grouped into two active SCS May-TC decades, namely, 1981-1990 and 2001-2010 and two inactive SCS May-TC decades: 1991-2000 and 2011-2020. A contrast analysis between the inactive decade 2011-2020 and the active decade 2001-2010 is discussed in CLS2022. In this study, we did the contrast analysis between the inactive decade 1991-2000 and the active decade 1981-1990 and compared the difference with the contrast after 2000. In addition, we use two leading EOF modes to objectively represent the seasonal transition. The EOF modes are calculated based on 40 years (1981-2020) of GPCP precipitation pentad data from March to June (pentad 13 to 37). EOF1 describes the northward movement of ITCZ from near the equator to the centers of the summer monsoon such as the ArS, BOB and SCS. EOF2 describes the westward movement of precipitation centers during the transition season from late-April to early-June, such as a wet and dry dipole pattern corresponding to the concurrent change over the equatorial eastern Indian Ocean and the western Pacific warm pool. It turns out that the decadal-scale SCS May-TC frequency is a good metric to capture the variability of monsoon transition. The higher TC frequency decade during 2001-2010 is also a decade with the earlier spring-to-summer transition suggested by PC1. Similar monsoon advancement is not found for the active SCS May-TC decade of 1981-1990. More active TC frequency during this decade is found to be associated with large and persistent positive PC2 during the critical transition time

from late-April to early-June (pentad 23-32). The EOF2 pattern is consistent with the large-scale environment difference that shows the weakened low-level westerlies (negative stream function) over the near-equatorial Indian Ocean and a long-stretched southeast-northwest high pressure pattern (positive stream function) from the Coral Sea to the northwest through New Guinea and Indonesia maritime continent to the BOB and the southern ArS.

4.2. *Discussion and concluding remarks*

The relationship between EOF2 and the climatological and transient intraseasonal oscillations is important to understand the spring-to-summer transition in particular over the SCS and the Philippine Sea and the vicinity area. The climatological intraseasonal oscillations (CISO) (Wang and Xu, 1997) have dynamically coherent structure including the organized convection and its low- and high-level associated convergent and divergent winds. The extreme phases of the CISOs were presented as monsoon singularities that occur on a fixed time of a year with usual regularity. During the period from May to October four CISO cycles were identified. The first cycle described as the northward shift of the pre-onset dry singularity of the South China Sea-Philippine summer monsoon (SCS-PSM) was characterized by a dry zone around 5° S that covered the eastern Indian Ocean and western part Indonesia islands on pentad 28 (16-20 May). The dry zone moved northeastward to 10° N on pentad 30 (26-30 May) that covered the SCS and the Philippine Sea. The peak wet phase of the first CISO cycle (6 May - 4 June) occurred in mid-May. The timing is near the climatological mean onset date of the SCSSM. Interestingly that the first CISO cycle is identifiable in the PC2 in Figs. 5(b&d). The time series of PC2 show during the decades of 1991-2000 and 2001-2010 two intensification episodes during the period from pentad 22 to pentad 34 (16 April-19 June). The second episode that shows a minimum around pentad 28 and maximum around pentad 32 matches the aforementioned first CISO very well in both temporal and spatial characteristics of the variations. During the SCS May-TC active decade (1981-1990) the second episode of the PC2 occurred earlier than that during the SCS May-TC inactive decade (1991-2000). Because the PC1 difference in these two decades is not discernable [Fig. 7(a)], the monsoon transition difference can be represented by the PC2. On the contrast, although Fig. 7(d) shows earlier monsoon transition in PC2 during the SCS May-TC inactive decade (2011-2020), the delayed monsoon transition signal in PC1 compared with the decade of 2001-2010 overwhelmed the PC2 signal.

MJO is the most prominent transient ISOs that can be an important influential factor to EOF2. We selected

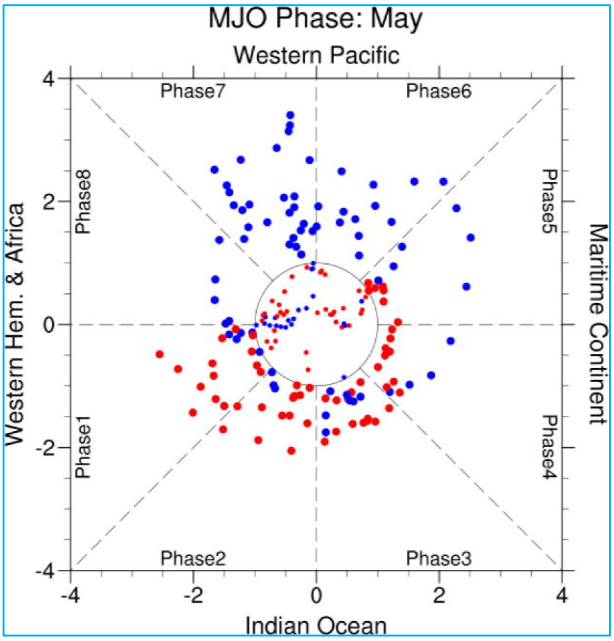

Fig. 9. MJO phase diagram with the daily MJO index values in May. The red dots indicate the three strongest years (1981, 1985, 2013) of accumulated amplitude PC2 from pentad 25 to 30 during 1981-2020. The blue dots indicate the three weakest years (1996, 2000, 2003)

three years (1981, 1985, 2013) with the strongest accumulated positive PC2 amplitude in May and three years (1996, 2000, 2003) with the weakest accumulated positive PC2 in May and mark the MJO RMM daily phase amplitude by different colors for the strong-positive (red) and weak-positive (blue) types of PC2. Fig. 9 shows that for the strong-positive PC2 type of May the MJO never appeared in phases 6-8. The MJO convection mainly appeared over the Indian Ocean and Indonesia maritime continent. For the weak-positive PC2 type of May, the MJO phase is mainly in phases 6-7. Those ones with phases 1-3 show relatively small amplitude. The results suggest that the BOB and SCS monsoon transition can be influenced by MJO. When the MJO convection is over the western Pacific or Indian Ocean in May the transition can be delayed or advanced. Further research is needed to delineate the relationship between MJO, CISO, SCSSM onset and the spring-to-summer transition of the ITCZ.

Our findings suggest that the spring-to-summer transition variability can be influenced by many factors. The difference between the inactive and active SCS May-TC decades shows the challenge in prediction the spring-to-summer transition in the vast Asian-Australian-Pacific monsoon region. Particular caution is required when applying the inter-decadal changes to project the future.

Acknowledgements

This study is supported by the Ministry of Science and Technology, Taiwan, Grant MOST 109-2811-M-002-646-MY2, MOST109-2111-M-002-005, MOST 110-2111-M-002-013, MOST 111-2111-M-002-007. CHS is supported by the grant MOST 109-2111-M-002-004, MOST 109-2119-M-001-011, MOST 110-2111-M-002-015, MOST 110-2119-M-002-012.

Disclaimer : The contents and views expressed in this study are the views of the authors and do not necessarily reflect the views of the organizations they belong to.

References

Chen, G., 2015, Comments on "Interdecadal change of the South China sea summer monsoon onset", *J. Climate*, **28**, 9029-9035. https://doi.org/10.1175/JCLI-D-14-00732.1.

Chen, W., Wang, L., Feng, J., Wen, Z., Ma, T., Yang, X. and Wang, C., 2019, "Recent progress in studies of the variabilities and mechanisms of the East Asian monsoon in a changing climate", *Adv. Atmos. Sci*., **36**, 887-901. https://doi.org/10.1007/s00376-019-8230-y.

Cho, Y. M. and Lu, M. M., 2017, "A downscaling Method for Predicting Taiwan Mei-yu Seasonal Extreme Rainfall Event Frequency Using a Large-Scale Southwest Flow Index", *Atmospheric Sciences*, **45**, 83-100. doi : 10.3966/025400022017064502001 (in Chinese with English abstract).

Cho, Y. M. and Lu, M. M., 2021, "Taiwan Mei-yu seasonal rainfall pattern and East Asian Summer Monsoon characteristics during the monsoon development stage", *Atmospheric Sciences*, **49**, 79-109. doi : 10.3966/025400022021074901004 (in Chinese with English abstract).

Cho, Y. M., Lu, M. M., Sui, C. H., Solis, A. L. and Chen, M. S., 2022, "Decadal changes of the early summer Asian monsoon and the South China Sea tropical cyclones during 2001-2020", *Terrestrial, Atmospheric and Oceanic Sciences*, **33**, 1, 1-20. https://link.springer.com/article/10.1007/s44195-022-00005-3.

Ding, Y. H. and Chen, J. C., 2005, "The East Asian summer monsoon: an overview", *Meteor. Atmos. Phys.*, **89**, 117-142. doi : 10.1007/s00703-005-0125-z.

Ding, Y., Liang, P., Liu, Y. J. and Zhang, Y. C., 2020, "Multiscale variability of Meiyu and its prediction : A new review", *J. Geophys. Res.*, **125(7)**, e2019JD031496. doi : 10.1029/2019JD031496.

Ding, Y., Liu, Y., Song, Y. and Zhang, J., 2015, "From MONEX to the global monsoon : A review of monsoon system research", *Adv. Atmos. Sci*., **32**, 10-31. https://doi.org/10.1007/s00376-014-0008-7.

Hersbach, H., Bell, B., Berrisford, P., Hirahara, S., Horányi, A. and Muñoz-Sabater, J., 2020, "The ERA5 global reanalysis", *Q. J. R. Meteorol. Soc.*, **146**, 1999-2049. doi : 10.1002/qj.3803.

Hu, P., Chen, W., Chen, S., Liu, Y., Wang, L. and Huang, R., 2022, "The leading mode and factors for coherent variations among the sub-systems of tropical Asian summer monsoon onset", *J. Climate*, **35**, 1597-1612. https://doi.org/10.1175/JCLI-D-21-0101.1.

Huang, B., Thorne, P. W., Banzon, V. F., Boyer, T., Chepurin, G., Lawrimore, J. H. , Menne, M. J., Smith, T. M., Vose, R. S. and Zhang, H. M., 2017, "Extended Reconstructed Sea Surface Temperature version 5 (ERSSTv5) : Upgrades, validations and intercomparisons", *J. Climate*, **30,** 20, 8179-8205. doi : 10.1175/JCLI-D-16-0836.1.

Huffman, G. J., Adler, R. F., Bolvin, D. T. and Gu, G., 2009, "Improving the global precipitation record : GPCP Version 2.1", *Geophys. Res. Lett.*, **36**, L17808. doi :10.1029/2009GL040000.

Kajikawa, Y. and Wang, B., 2012, "Interdecadal Change of the South China Sea Summer Monsoon Onset", *J. Climate*, **25**, 9, 3207-3218. doi : 10.1175/JCLI-D-11-00207.1.

Kajikawa, Y., Yasunari, T., Yoshida, S. and Fujinami, H., 2012, "Advanced Asian summer monsoon onset in recent decades", *Geophys. Res. Lett*., **39**, L03803. doi : 10.1029/2011GL050540.

Lau, K. M. and Kim, K.M., 2006, "Observational relationships between aerosol and Asian monsoon rainfall and circulation", *Geophys. Res. Lett.*, **33**, L21810. doi :10.1029/2006GL027546.

Lau, K. M., 1992, "East Asian summer monsoon rainfall variability and climate teleconnection", *J. Meteor. Soc. Japan*, **70(1B)**, 211-242. doi : 10.2151/jmsj1965.70.1B_211.

Lau, K. M., Kim, M. K. and Kim, K. M., 2006, "Asian summer monsoon anomalies induced by aerosol direct forcing : The role of the Tibetan Plateau", *Clim. Dyn*., **26**, 855-864. doi : 10.1007/s00382-006-0114-z.

Lee, H. T. and NOAA CDR Program, 2011, "NOAA Climate Data Record (CDR) of Daily Outgoing Longwave Radiation (OLR), Version 1.2", NOAA National Climatic Data Center. doi : 10.7289/V5SJ1HH2.

Lin, A. and Zhang, R. 2020, "Climate shift of the South China Sea summer monsoon onset in 1993/1994 and its physical causes", *Climate Dyn*., **54**, 1819-1827. https://doi.org/10.1007/s00382-019-05086-4.

Liu, B., Zhu, C., Yuan, Y. and Xu, K., 2016, "Two types of interannual variability of South China Sea monsoon onset related to the SST anomalies before and after 1993/94", *J. Climate*, **29**, 6957-6958. doi : 10.1175/JCLI-D-16-0065.1.

Lu, M. M., Sui, C. H., Sun J. R. and Lin, P. H., 2020, "Influences of subseasonal to interannual oscillations on the SCS summer monsoon onset in 2018", *Terr. Atmos. Ocean. Sci.*, **31**, 2, 197-209. doi : 10.3319/TAO.2020.02.25.01.

Lyon, B., Barnston, A. G. and De Witt, D. G., 2014, "Tropical Pacific forcing of a 1998-1999 climate shift: Observational analysis and climate model results for the boreal spring season", *Clim. Dyn.*, **43**, 3-4, 893-909. doi : 10.1007/S00382-013-1891-9.

Tu, J. Y., Chou, C., Huang, P. and Huang, R., 2011, "An abrupt increase of intense typhoons over the western North Pacific in early summer", *Environ. Res. Lett*., **6**, 3, 034013. doi : 10.1088/1748-9326/6/3/034013.

Wang, B. and Kajikawa, Y., 2015, "Reply to "Comments on 'Interdecadal change of the South China Sea summer monsoon onset", *J. Climate*, **28**, 9036-9039, https://doi.org/10.1175/JCLI-D-15-0173.1.

Wang, B. and LinHo, 2002, "Rainy Season of the Asian-Pacific Summer Monsoon",*J. Climate*, **15**, 4, 386-398. doi : 10.1175/1520-0442(2002)015<0386:RSOTAP>2.0.CO;2.

Wang, B. and Xu, Xihua, 1997, "Northern Hemisphere summer monsoon singularities and climatological intraseasonal oscillation", *J. Climate*, **10**, 1071-1085. https://doi.org/10.1175/1520-0442(1997)010<1071:NHSMSA>2.0.CO;2.

Wang, B., Wu, R. and Lau, K. M., 2001, "Interannual variability of the Asian summer monsoon: Contrasts between the Indian and the western North Pacific-East Asian monsoons", *J. Climate*, **14**, 20, 4073-4090. doi : 10.1175/1520-0442(2001)014<4073: IVOTAS>2.0.CO;2.

Xiang, B. and Wang, B., 2013, "Mechanisms for the Advanced Asian Summer Monsoon Onset since the Mid-to-Late 1990s", *J. Climate*, **26**, 6, 1993-2009. doi : 10.1175/JCLI-D-12-00445.1.

Xu, S. and Wang, B., 2014, "Enhanced western North Pacific tropical cyclone activity in May in recent years", *Clim. Dyn.*, **42**, 9-10, 2555-2563. doi : 10.1007/s00382-013-1921-7.

Yuan, F. and Chen, W., 2013, "Roles of the tropical convective activities over different regions in the earlier onset of the South China Sea summer monsoon after 1993", *Theor. Appl. Climatol.*, **113**, 175-185. https://doi.org/10.1007/s00704-012-0776-x.